Journal of Radiation Research, Vol. 58, No. 5, 2017, pp. 675–684
doi: 10.1093/jrr/rrw129
Advance Access Publication: 13 February 2017

Organ-specific modulation complexity score for the evaluation of dose delivery

Iori Sumida[1,*], Hajime Yamaguchi[2], Indra J. Das[3], Hisao Kizaki[2], Keiko Aboshi[2], Mari Tsujii[2], Yuji Yamada[2], Keisuke Tamari[1], Yuji Seo[1], Fumiaki Isohashi[1], Yasuo Yoshioka[1] and Kazuhiko Ogawa[1]

[1]Department of Radiation Oncology, Osaka University Graduate School of Medicine, 2-2 Yamada-oka, Suita, Osaka, 565-0871, Japan
[2]Department of Radiation Oncology, NTT West Osaka Hospital, 2-6-40 Karasugatsuji, Tennoji-ku, Osaka, 543-8922, Japan
[3]Department of Radiation Oncology, New York University Langone Medical Center, 160 E 34th Street, New York, NY 10016, USA
*Corresponding author. Department of Radiation Oncology, Graduate School of Medicine, Osaka University, 2-2 Yamada-oka, Suita, Osaka, 565-0871 Japan. Tel: +81-6-6879-3482; Fax: +81-6-6879-3489; Email: sumida@radonc.med.osaka-u.ac.jp
Received July 6, 2016; Revised November 12, 2016; Editorial Decision December 18, 2016

ABSTRACT

The purpose of this study was to correlate the modulation complexity score (MCS) with organ location and to predict potential dose errors for organs before beam delivery for intensity-modulated radiation therapy (IMRT) dosimetry. Sixteen head and neck cancer patients treated with IMRT were selected. Distribution of the relative dose error on each beam was performed using forward projection to the planned dose to compute the predicted dose after doing per-beam quality assurance. Original organ-specific modulation complexity score (oMCS) was created based on a modified MLC, which depended on organ location. First, MCS was calculated based on the change in leaf position between adjacent MLC leaves. Second, the segment edge map (SEM) calculated from the intensity map for each beam was applied to the calculation volume. The oMCS with segment edge ($oMCS_{edge}$) was derived from the product of oMCS and SEM. The correlation between the dose errors (planned and predicted) and $oMCS_{edge}$ values was evaluated for the target and organs at risk. We have also expanded the original MCS concept to $oMCS_{edge}$ including the organ location. We observed a moderate correlation between the dose errors and $oMCS_{edge}$ for all organs and volumes of interest except the gross tumor volume, brain stem, and spinal cord. In other organs, a moderate improvement in sensitivity was observed on the SEM, which was correlated with dose errors. Although the implementation of $oMCS_{edge}$ would be impractical for normal clinical settings, it is expected that $oMCS_{edge}$ would help a treatment planner to judge whether or not the treatment plan would be acceptably delivered.

KEYWORDS: IMRT, dose prediction, plan complexity, beam deliverability, quality assurance

INTRODUCTION

Intensity-modulated radiation therapy (IMRT) creates a steep dose gradient at the interface of the target and organs at risk (OARs). Dose distributions are optimized based on dose–volume constraints and calculated using modern dose calculation algorithms; however, dose delivery may still be uncertain in terms of the accuracy of dose calculation for a treatment machine by the treatment planning system (TPS). The discrepancies between the planned and measured dose are evaluated by the gamma passing rate [1] and the composite analysis [2] for both dose difference and distance-to-agreement as a patient-specific quality assurance (QA).

The modulation complexity score (MCS) described by McNiven *et al.* [3] represents the plan complexity using the following parameters: positions of leaf, degree of irregularity in field shape, weight of the segment, and area. Their study measured the correlation between MCS and QA dose delivery as measured by the 2D diode array in terms of beam parameters such as the number of segments and monitor units (MUs). Several authors [4–7] have reported the correlation between MCS and the gamma passing rate in volumetric modulated arc therapy (VMAT) from the viewpoint of plan deliverability. The original MCS concept deals with plan deliverability based on the variability of leaf positions and aperture

areas between segments. It provides the plan complexity as a single value from 1 (for simple) to 0 (for complex). However, its correlation with organ locations has not been studied.

Recently, the measurement-guided dose reconstruction (MGDR) approach has been applied [8, 9]. It incorporates data captured by 2D or 3D detectors into the treatment plan, i.e. it predicts dose distribution along with dose delivery errors based on patient-specific QA. The approach involves the evaluation of dose delivery based on dose–volume histograms (DVHs).

The purpose of this study was to extend the concept of MCS to include the complexity of beam delivery to a specified organ. The new concept, organ-specific MCS (oMCS), is demonstrated using the MGDR approach for head and neck (H&N) cancer. The motivation for this study was in the context of correlation between the oMCS value and the predicted potential dose errors for organs, using the MGDR approach. Although the implementation for calculation of the oMCS value needs special software, making it impractical for normal clinical settings, it is expected that the oMCS value will be able to help a treatment planner in deciding whether re-planning by change of dose constraints for organs is necessary; this would help with modification of the plan so that it was made more robust against dosimetric uncertainty for beam delivery.

MATERIALS AND METHODS

Treatment plan

Sixteen H&N cancer patients who were treated with IMRT were selected. A linear accelerator equipped with a 6 MV photon beam (ONCOR Impression PLUS; Siemens Medical Systems, Concord, CA) was used. Fixed gantry step-and-shoot IMRT with a 1-cm leaf width was used for irradiation. The gross tumor volume (GTV) and the clinical target volume (CTV) including elective lymph nodes were expanded by a 5-mm margin to create the volumes of interest called PTV_{70Gy} and PTV_{56Gy} that received 70 Gy and 56 Gy in 35 fractions, respectively. The prescription doses were 2 Gy per fraction and 1.6 Gy per fraction for the PTV_{70Gy} and PTV_{56Gy}, respectively. Planning organ at risk volumes (PRVs) were created by adding a 3-mm margin to the brain stem and a 5-mm margin to the spinal cord, respectively. The XiO (Elekta AB, Stockholm, Sweden) TPS was used to calculate dose distribution with a 2-mm grid resolution. The dose–volume constraints were as follows: maximum dose of <54 Gy and <45 Gy for the brain stem and spinal cord, respectively. For the parotid gland, the percentage volume receiving 26 Gy (V_{26Gy}) was <50%.

Dose prediction with the MGDR approach

The concept of MGDR was proposed by Sumida *et al.* [9]. Briefly, after the original treatment plan was superimposed onto the water-equivalent phantom at a 5-cm depth and 100-cm source–axis distance at gantry 0° (which was different from the treatment beam angle), the measured dose distribution was acquired by a MapCHECK 2D diode array (Sun Nuclear, Melbourne, FL). A relative dose error map was created by comparing the calculated and measured dose distributions using in-house software developed by Delphi2007® (Borland Software Corporation, Austin, TX). The grid resolution was 1 × 1 mm^2 and 5 × 5 mm^2 in the TPS and the 2D diode array, respectively. By forward projection, the relative dose error map in 2D was adopted into the dose grid in 3D for the corresponding beam to reconstruct the predicted dose distribution. The forward projection was repeated for each treatment beam. The 3D dose grid was exported from the TPS in the DICOM-RT format. The ray from the source to each dose grid was defined, and the intersection point on the relative dose error map located in the isocenter plane was calculated. The intersection point was calculated by 2D linear interpolations. The relative error was applied to each dose grid along the ray.

MCS with segment edge, oMCS

MCS expresses the plan complexity with respect to three parameters: segment shape, area and weight. The leaf sequence variability (LSV) parameter has been used to describe the variability in segment shape, and the aperture area variability (AAV) has been used to describe the variation in segment area relative to the maximum aperture defined by all segments. MCS ranges from 1 to 0. A score of 1 means no modulation, such as that in a rectangular target field, whereas for more complex treatment plans, MCS becomes close to 0.

The original calculation of MCS was followed as defined by McNiven [3]. First, the maximum distance between positions for a leaf bank is defined as follows:

$$pos_{max} = \left\langle max\left(pos_{n\in N}\right) - min\left(pos_{n\in N}\right)\right\rangle_{leaf\ bank}, \qquad (1)$$

where N is the number of open leaves that constitute the segment beam, *pos* is the leaf position in the form of coordinates, and n starts from 1. An example of the MLC leaf positions in a segment is shown in Fig. 1, where N is 21.

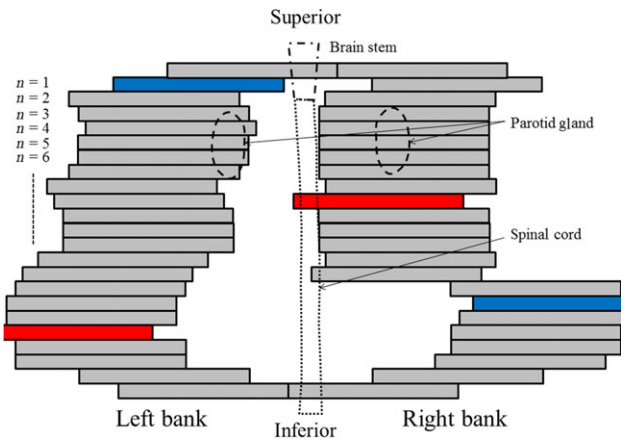

Fig. 1. Examples of certain segment shapes and organ contours. The extreme right and extreme left leaves in the left leaf bank are in blue and red, respectively. The extreme right and extreme left leaves in the right leaf bank are in blue and red, respectively. The maximum leaf opening was observed in the red leaf in the left bank and in the blue leaf in the right bank.

The extreme left and right leaves in each leaf bank represent $min(pos_{n\in N})$ and $max(pos_{n\in N})$ (red and blue, respectively). The notation pos_{max} is the maximum change between $max(pos_{n\in N})$ and $min(pos_{n\in N})$. LSV in each segment represents the complexity of segment shape, which is reflected in the change in leaf position between adjacent MLC leaves (n and $n + 1$) with respect to pos_{max}. The equation is defined as follows:

$$LSV_{seg} = \left\langle \frac{\sum_{n=1}^{N-1}\left(pos_{max} - |pos_n - pos_{n+1}|\right)}{(N-1)\times pos_{max}} \right\rangle_{left\ bank} * \left\langle \frac{\sum_{n=1}^{N-1}\left(pos_{max} - |pos_n - pos_{n+1}|\right)}{(N-1)\times pos_{max}} \right\rangle_{right\ bank.} \quad (2)$$

To consider the organ location in each sector in the superior-inferior (SI) direction to LSV_{seg}, the sectored LSV_{seg} ($sLSV_{seg}$) was calculated for each adjacent leaf, which implies that the combination of adjacent leaf pairs was $n = 1$ and 2, $n = 2$ and 3, $n = 3$ and 4, and so on as shown in Fig. 1. For example, the parotid glands correspond to the leaf pairs between 3 and 7, and the spinal cord corresponds to the leaf pairs between 2 and 21, respectively (Fig. 1).

Second, the segment characteristics considered the complexity of beam delivery is the area of the segment opening. AAV is calculated using the following equation:

$$AAV_{seg} = \frac{\sum_{n=1}^{N}\left(\langle pos_n\rangle_{left\ bank} - \langle pos_n\rangle_{right\ bank}\right)}{N\times\left(\langle max(pos_n)\rangle_{left\ bank\in segment} - \langle max(pos_n)\rangle_{right\ bank\in segment}\right)}, \quad (3)$$

where $\langle max(pos_n)\rangle_{left\ bank\in segment}$ and $\langle max(pos_n)\rangle_{right\ bank\in segment}$ are the maximum opening position leaves shown in Fig. 1 in red.

Finally, the segment weight in a beam is considered as a relative impact to the complexity. MCS_{beam} is the product of LSV_{seg} and AAV_{seg}, and the relative weight of the segment in a beam is expressed as follows:

$$MCS_{beam} = \sum_{i=1}^{I}\left(LSV_{i-th\ seg}\times AAV_{i-th\ seg}\times\frac{MU_{i-th\ seg}}{MU_{beam}}\right), \quad (4)$$

where I is the number of segments in the beam. Although the original MCS is as expressed in Eq. (4), $sLSV_{seg}$ used in this study was applied to Eq. (4) to calculate oMCS as follows:

$$oMCS_{beam} = \sum_{i=1}^{I}\left(sLSV_{i-th\ seg}\times AAV_{i-th\ seg}\times\frac{MU_{i-th\ seg}}{MU_{beam}}\right). \quad (5)$$

The total plan complexity is defined by $oMCS_{plan}$, i.e. $oMCS_{beam}$ weighted by the relative MU of each beam ($MU_{k-th\ beam}$) in the plan expressed as follows:

$$oMCS_{plan} = \sum_{k=1}^{K}\left(oMCS_{k-th\ beam}\times\frac{MU_{k-th\ beam}}{MU_{plan}}\right), \quad (6)$$

where K is the number of beams in the plan and MU_{plan} refers to the total MU in the plan.

To consider the modulation complexity for an organ in step-and shoot IMRT planning, the information of organ located in the SI direction has been previously considered. However the information is limited to one direction; therefore, we propose the segment edge map (SEM) as a new factor for improving the sensitivity for the complexity and to consider where the gradient change of the beam intensity along the leaf motion should occur, taking into account the organ location in three dimensions. Because SEM has a steep dose gradient, we have presumed that the segment edge may result in a potential dose difference due to the MLC leaf positional error, the leaf end transmission beam data for dose calculation, and the detector density of the 2D diode array for dose distribution measurement. Younge *et al.* [10] reported that the majority of the dose differences are concentrated at the edges of the aperture defined by the MLC leaves.

SEM was calculated from the DICOM RT-plan file. First, 2D matrices of 400 × 400 mm^2 in 1-mm resolution were defined and placed at a source–axis distance of 100 cm. Using the segment shape and its MUs in the beam recorded in the DICOM RT-plan file, the MU-based intensity map was created as shown in Fig. 2a.

Subsequently, the map was scanned for 1 mm each along the MLC leaf motion to detect the edge intensity and normalized to the maximum MUs (intensity) in the beam. Finally, the edge intensity map was weighted by the relative MUs of each beam

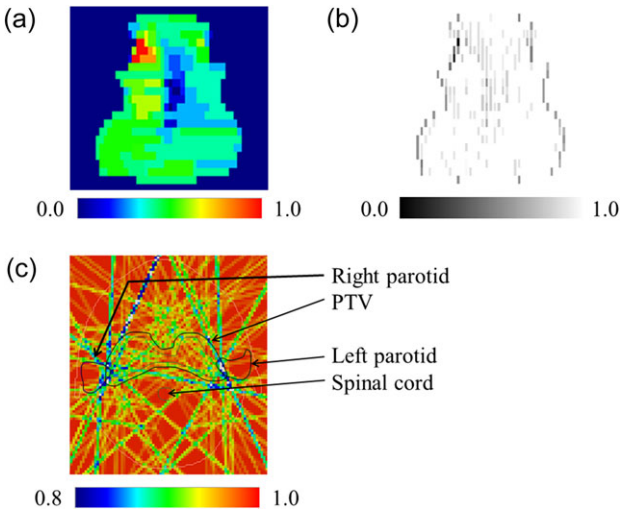

Fig. 2. (a) MU-based intensity map, (b) segment edge distribution calculated from the MU-based intensity map, and (c) the segment edge volume distribution in the axial plane. Red denotes the maximum intensity and blue the minimum intensity (Fig 2a). The dark black denotes a steep intensity difference and light black denotes a low intensity difference (2b). In Fig. 2c, the grid in red receives no segment edge and that in blue receives segment edges. The grid that receives more segment edges will change in blue color. The color bar represents the range (0.8–1.0) of the segment edge volume. MU = monitor units, PTV = planning target volume.

($MU_{k-th\ beam}$) in the plan. The SEM_{beam} was calculated by the following equation:

$$SEM_{k-th\ beam}(i,j) = \frac{|MU(i,j) - MU(i+1,j)|}{max(MU_{k-th\ beam})} \times \frac{MU_{k-th\ beam}}{MU_{plan}},$$

$$if |MU(i,j) - MU(i+1,j)| \neq 0\ then$$

$$SEM_{k-th\ beam}(i-1,j) = SEM_{k-th\ beam}(i,j) = SEM_{k-th\ beam}(i+1,j), \quad (7)$$

where i denotes the coordinates of the MLC leaf motion and j denotes the coordinates perpendicular to the MLC leaf motion. After the segment edge was detected, the SEM value was then applied to the neighboring location with ± 1 mm. Figure 2b shows an SEM distribution. As the dose grid resolution used was 2 mm each and when the gantry angle for the MGDR approach was 45°, the corresponding dose grid width would be 2.8 mm. As shown in Fig. 2b, the segment edge width would be 3 mm. Using the same procedure as described for dose prediction with the MGDR approach, SEM in 2D was adopted into the same grid as the dose grid used in 3D of the corresponding beam to reconstruct the segment edge volume (SEV). In other words, the SEV grid would consist of the same number of grids as the dose grid (x, y, z); the value of the grid was initialized to 0. The forward projection was repeated for each treatment beam. To reconstruct SEV, the following equation was used:

$$SEV_{x,y,z} = \sum_{k=1}^{K} (SEV_{x,y,z} + SEM_{k-th\ beam}(i,j)). \quad (8)$$

Figure 2c shows a sample SEV distribution in the axial plane. According to Eqs (7) and (8), the SEV of the grid at which none of the beams hit the segment edge would correspond to the one shown in red in Fig. 2c. In case the grid was hit by more segment edges, the corresponding SEV would be <1 (indicated in blue at the overlap region between the right parotid and the PTV in Fig. 2c). As applicable to MCS, the grid with the lower SEV is susceptible to dose errors.

Finally, oMCS was combined with the grid value of SEV to create a new index called $oMCS_{edge}$ using the following equation:

$$oMCS_{edge} = oMCS_{plan} \times SEV_{x,y,z}. \quad (9)$$

Correlation between dose error and $oMCS_{edge}$

The discrepancies between the planned and predicted doses delivered at the target and at OARs in 16 patients were evaluated. These organs were GTV, CTV, PTV_{70Gy}, PTV_{56Gy}, brain stem, PRV brain stem, spinal cord, PRV spinal cord, and both parotid glands. The dose–volume parameters of $D_{2\%}$ in Gy as a maximum dose, $D_{98\%}$ in Gy as a minimum dose, mean dose in Gy, and homogeneity index (HI) were calculated for all organs. HI was defined as $(D_{2\%} - D_{98\%})/D_{50\%}$, as discussed in International Commission on Radiation Units and Measurements report 83 [11].

As the $oMCS_{edge}$ has been derived from the $sLSV_{segment}$ in the SI direction, the organ volumes were split into sectors, each with a 1-cm width, depending on the MLC leaf width in the SI direction; following this, dose errors in the sectors were calculated. For example, the right parotid corresponds to leaves 3 to 7 (shown in Fig. 1). The dose error for the sector volume in the right parotid was calculated as the root mean square errors (RMSEs) between the planned and predicted doses. Regarding other organs, RMSEs were also calculated in each sector. For the $oMCS_{edge}$, the SEV grid belongs to the corresponding organ; therefore, the $oMCS_{edge}$ value was calculated in each sector along the SI direction for each organ. Subsequently, the correlation between the dose error and the $oMCS_{edge}$ for each organ was drawn.

As described above, the correlation between RMSE and the $oMCS_{plan}$ for each organ was also drawn to compare the correlation coefficients with or without SEM (i.e. $oMCS_{plan}$ and $oMCS_{edge}$).

Correlation between the gamma passing rate and MCS, the number of segments, and total monitor units

The 3D gamma evaluation [12] for the discrepancy between the planned and predicted dose distributions, and the gamma passing rate was calculated within tolerance limits of 3% global/3 mm and 2% global/2 mm. 'Global' refers to the global normalization to the prescription dose. The dose evaluation region was defined as dose per voxel (dose grid) of >10% of the prescribed dose. After the 3D gamma evaluation, the correlations between the gamma passing rate and MCS, the number of segments, and total MUs were further examined.

Statistical analysis

The Shapiro–Wilk test was performed to check the normality of the data; for correlation analysis, either Pearson's or Spearman's correlation coefficient (r) was selected depending on the normality. Statistical analyses were performed using R version 3.1.2 statistical software (R Foundation, Vienna, Austria). The correlation coefficients for two dependent samples ($oMCS_{plan}$ and $oMCS_{edge}$) with respect to RMSEs for the organs were analyzed using the methodology proposed by Steiger [13]. A P-value of <0.05 was considered indicative of a statistically significant difference.

RESULTS

The dose–volume indices for the planned and predicted doses are summarized in Table 1. The $D_{2\%}$, $D_{98\%}$, and the mean dose in the predicted dose for the GTV, CTV, PTV_{70Gy} and PTV_{56Gy} were significantly smaller than those in the planned dose. The dose discrepancies were <1 Gy for most organs; however, those of $D_{98\%}$ for the PTV_{70Gy} and PTV_{56Gy} were 1.8 Gy and 1.6 Gy, respectively. HI of the GTV and CTV for the planned and predicted doses were not significantly different. In contrast, the HI of the PTV_{70Gy} and PTV_{56Gy} for the predicted dose were significantly larger than those for the planned dose. $D_{2\%}$ of brain stem and PRV brain stem for the planned and predicted doses were not significantly different. $D_{2\%}$ of spinal cord for the predicted dose was significantly larger than that for the planned dose. In contrast, $D_{2\%}$ of the PRV spinal cord for the planned and predicted doses was not significantly different. The mean doses of both parotids for the predicted dose were significantly larger than those for the planned dose.

Table 1. Comparisons of the volume indices between the planned and predicted dose distributions determined for 16 cases with head and neck cancer

Index	Planned dose	Predicted dose	*P*-value
GTV $D_{2\%}$ (Gy)	72.57 ± 0.72	72.04 ± 0.62	<0.003
GTV $D_{98\%}$ (Gy)	67.71 ± 1.24	66.73 ± 1.16	<0.001
GTV mean dose (Gy)	70.62 ± 0.26	70.07 ± 0.50	<0.001
GTV HI	0.07 ± 0.02	0.08 ± 0.02	NS
CTV $D_{2\%}$ (Gy)	71.55 ± 0.74	70.77 ± 0.85	<0.001
CTV $D_{98\%}$ (Gy)	53.28 ± 0.85	52.76 ± 1.08	<0.001
CTV mean dose (Gy)	60.57 ± 1.68	60.16 ± 1.69	<0.001
CTV HI	0.31 ± 0.01	0.31 ± 0.02	NS
PTV_{70Gy} $D_{2\%}$ (Gy)	72.58 ± 0.60	71.80 ± 0.58	<0.001
PTV_{70Gy} $D_{98\%}$ (Gy)	64.95 ± 0.91	63.20 ± 1.50	<0.001
PTV_{70Gy} mean dose (Gy)	69.89 ± 0.13	68.79 ± 0.62	<0.001
PTV_{70Gy} HI	0.11 ± 0.02	0.12 ± 0.02	<0.02
PTV_{56Gy} $D_{2\%}$ (Gy)	62.00 ± 1.17	61.73 ± 1.07	<0.02
PTV_{56Gy} $D_{98\%}$ (Gy)	49.53 ± 1.05	47.92 ± 1.19	<0.001
PTV_{56Gy} mean dose (Gy)	56.61 ± 0.32	56.20 ± 0.36	<0.001
PTV_{56Gy} HI	0.22 ± 0.03	0.25 ± 0.03	<0.001
Brain stem $D_{2\%}$ (Gy)	38.83 ± 1.84	39.23 ± 2.04	NS
Brain stem $D_{98\%}$ (Gy)	6.18 ± 5.69	8.49 ± 5.45	<0.003
Brain stem mean dose (Gy)	25.78 ± 4.17	26.27 ± 3.69	NS
Brain stem HI	1.26 ± 0.69	1.16 ± 0.49	<0.04
PRV brain stem $D_{2\%}$ (Gy)	40.23 ± 2.31	40.72 ± 2.34	NS
PRV brain stem $D_{98\%}$ (Gy)	6.14 ± 5.60	8.53 ± 5.42	<0.005
PRV brain stem mean dose (Gy)	26.51 ± 4.18	26.95 ± 3.74	NS
PRV brain stem HI	1.27 ± 0.67	1.17 ± 0.45	<0.02
Spinal cord $D_{2\%}$ (Gy)	39.27 ± 1.49	39.72 ± 1.73	<0.04
Spinal cord $D_{98\%}$ (Gy)	0.84 ± 0.51	1.28 ± 1.21	<0.05
Spinal cord mean dose (Gy)	28.44 ± 2.42	29.28 ± 2.55	<0.001
Spinal cord HI	1.14 ± 0.04	1.12 ± 0.05	<0.04
PRV spinal cord $D_{2\%}$ (Gy)	41.38 ± 1.34	41.75 ± 1.56	NS
PRV spinal cord $D_{98\%}$ (Gy)	0.83 ± 0.49	1.24 ± 1.22	NS
PRV spinal cord mean dose (Gy)	29.37 ± 2.39	30.09 ± 2.53	<0.001
PRV spinal cord HI	1.17 ± 0.04	1.15 ± 0.06	NS

Continued

Table 1. Continued

Index	Planned dose	Predicted dose	*P*-value
Left parotid $D_{2\%}$ (Gy)	62.56 ± 5.92	61.68 ± 5.74	<0.001
Left parotid $D_{98\%}$ (Gy)	9.62 ± 3.29	11.59 ± 3.24	<0.001
Left parotid mean dose (Gy)	30.42 ± 3.61	32.65 ± 3.59	<0.001
Left parotid HI	2.29 ± 0.30	1.84 ± 0.19	<0.001
Right parotid $D_{2\%}$ (Gy)	56.61 ± 9.62	55.97 ± 9.42	<0.003
Right parotid $D_{98\%}$ (Gy)	9.98 ± 3.38	11.79 ± 4.00	<0.001
Right parotid mean dose (Gy)	28.60 ± 5.32	30.44 ± 5.82	<0.001
Right parotid HI	2.10 ± 0.34	1.76 ± 0.30	<0.001

GTV = gross tumor volume, CTV = clinical target volume, PTV_{xGy} = the percentage of planning target volume receiving *x* Gy, PRV = planning organ at risk volume, $D_{x\%}$ = the absorbed dose received by *x*% of the volume, HI = homogeneity index, NS = not significant. Values are means ± SD.

Table 2. Correlation between the root mean square errors for the planned and predicted doses and organ-specific modulation complexity score with segment edge map at the target and organs at risk in 16 cases of head and neck cancer

Organ	$oMCS_{plan}$	SEV	$oMCS_{edge}$	RMSE (%)	Correlation coefficient (*r*)	*P*-value
GTV	0.189 ± 0.045	0.975 ± 0.013	0.184 ± 0.044	1.40 ± 0.89	−0.244	<0.02
CTV	0.174 ± 0.052	0.973 ± 0.015	0.169 ± 0.051	1.76 ± 1.40	−0.497	<0.001
PTV_{70Gy}	0.186 ± 0.045	0.972 ± 0.013	0.181 ± 0.043	2.09 ± 1.52	−0.224	<0.02
PTV_{56Gy}	0.170 ± 0.055	0.971 ± 0.016	0.165 ± 0.054	1.92 ± 1.62	−0.538	<0.001
Brain stem	0.123 ± 0.051	0.972 ± 0.014	0.119 ± 0.049	2.58 ± 1.64	−0.411	<0.001
PRV brain stem	0.123 ± 0.051	0.969 ± 0.014	0.119 ± 0.048	2.66 ± 1.62	−0.436	<0.001
Spinal cord	0.181 ± 0.053	0.968 ± 0.017	0.174 ± 0.051	1.52 ± 1.07	−0.317	<0.001
PRV spinal cord	0.181 ± 0.053	0.962 ± 0.016	0.174 ± 0.050	1.54 ± 0.96	−0.338	<0.001
Left parotid	0.169 ± 0.057	0.949 ± 0.024	0.160 ± 0.055	3.92 ± 2.20	−0.379	<0.001
Right parotid	0.167 ± 0.058	0.953 ± 0.022	0.159 ± 0.055	3.43 ± 2.07	−0.456	<0.001

$oMCS_{plan}$ = organ-specific modulation complexity score without segment edge map, SEV = segment edge volume reconstructed from the segment edge map, $oMCS_{edge}$ = organ-specific modulation complexity score with segment edge map, RMSE = root mean square error, GTV = gross tumor volume, CTV = clinical target volume, PTV_{xGy} = the percentage of planning target volume receiving *x* Gy, PRV = planning organ at risk volume. Values are means ± SD.

$oMCS_{plan}$ and the SEV reconstructed from the SEM for the target and OARs are shown in Table 2. Again, $oMCS_{edge}$ was calculated based on $oMCS_{plan}$ and SEV as shown in Eq. (9). Correlation between the RMSEs for the planned and predicted doses and $oMCS_{edge}$ in the target and OARs is shown in Table 2 and Fig. 3. Blue markers shown in Fig. 3 correspond to the dose grids in the organs. Black lines represent the linear regression of the correlation coefficients. Moderate negative correlations were found in all organs ($P < 0.02$ or 0.001). Correlation coefficients were −0.244, −0.497, −0.224, −0.538, −0.411, −0.436, −0.317, −0.338, −0.379 and −0.456 for GTV, CTV, PTV_{70Gy}, PTV_{56Gy}, the brain stem, the PRV brain stem, the spinal cord, the PRV spinal cord, the left parotid and the right parotid, respectively. As can be seen, the smaller the $oMCS_{edge}$ value, the larger is RMSE. RMSEs for both parotids were relatively higher (>3%) than those for other organs.

The comparison of the correlation coefficient between $oMCS_{plan}$ and $oMCS_{edge}$ with respect to RMSEs between the planned and predicted doses in the target and OARs are shown in Table 3. A statistically moderate difference was observed between $oMCS_{plan}$ and $oMCS_{edge}$ for the CTV ($P < 0.001$), PTV_{70Gy} ($P < 0.01$), PTV_{56Gy} ($P < 0.001$), the left parotid ($P < 0.001$) and the right parotid ($P < 0.001$). Stronger and more negative correlations were found between $oMCS_{edge}$ and $oMCS_{plan}$. As an example, the correlation between the RMSEs and scores of $oMCS_{plan}$ or $oMCS_{edge}$ for

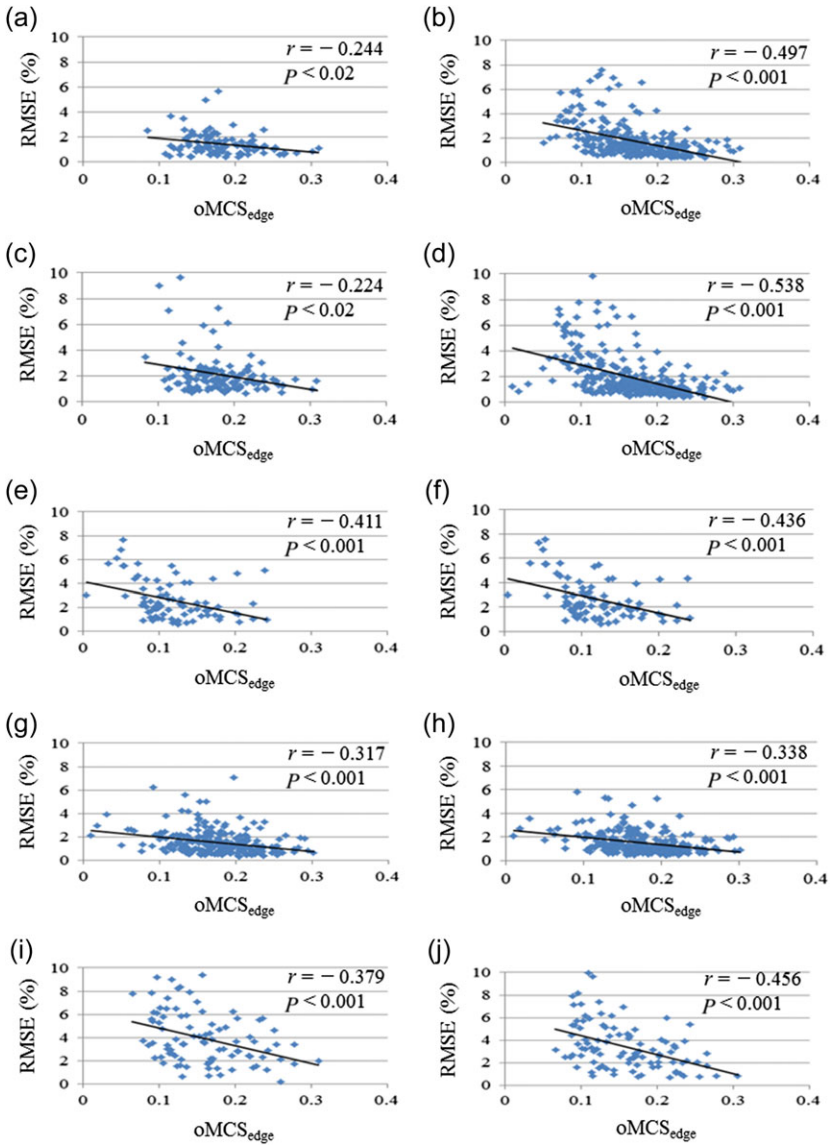

Fig. 3. Scatter plots showing correlation between RMSEs for the planned and predicted doses and oMCS$_{edge}$ in the target and OAR: (a) GTV, (b) CTV, (c) PTV$_{70Gy}$, (d) PTV$_{56Gy}$, (e) brain stem, (f) PRV brain stem, (g) spinal cord, (h) PRV spinal cord, (i) right parotid and (j) left parotid. The regression coefficients and associated *P*-values are shown.

the right parotid is depicted in Fig. 4. Markers correspond to the dose grids. Black lines represent the linear regression with the correlation coefficients. No significant difference was observed with respect to other organs (GTV, the brain stem, the PRV brain stem, the spinal cord and the PRV spinal cord).

Correlation between the gamma passing rates for the 3% global/3 mm and 2% global/2 mm criteria and the MCS, the number of segments, and total MUs for 16 cases are shown in Fig. 5. The gamma passing rates were 95.4% and 85.9% for the 3% global/3 mm and 2% global/2 mm criteria, respectively. The mean and standard deviation of the MCS, the number of segments, and the total MUs were 0.383 ± 0.036, 169 ± 32, and 761 ± 134, respectively. Correlations between the number of segments and the MUs and the gamma passing rates under 2% global/2 mm criteria were found. The larger were the number of segments and the MUs, the smaller were the gamma passing rates. In contrast, there was no correlation of the gamma passing rates under the 3% global/3 mm and 2% global/2 mm criteria and the other indices.

DISCUSSION

The MCS incorporates the segment shape, segment area and segment weight to represent the plan complexity for any beam delivery technique (step-and-shoot, sliding window, and VMAT) for any organ [3]. MCS recognizes the plan complexity for total beam delivery; therefore, in this study we have referred to the original MCS

Table 3. Correlation coefficient for $oMCS_{plan}$ and $oMCS_{edge}$ with respect to the root mean square errors between the planned and predicted doses at the target and at organs at risk in 16 cases of head and neck cancer

Organ	Correlation coefficient (r)		P-value
	$oMCS_{plan}$	$oMCS_{edge}$	
GTV	−0.237	−0.244	NS
CTV	−0.472	−0.497	<0.001
PTV_{70Gy}	−0.209	−0.224	<0.01
PTV_{56Gy}	−0.519	−0.538	<0.001
Brain stem	−0.406	−0.411	NS
PRV brain stem	−0.432	−0.436	NS
Spinal cord	−0.312	−0.317	NS
PRV spinal cord	−0.337	−0.338	NS
Left parotid	−0.350	−0.379	<0.001
Right parotid	−0.431	−0.456	<0.001

$oMCS_{plan}$ = organ-specific modulation complexity score of the plan, $oMCS_{edge}$ = organ-specific modulation complexity score with segment edge, GTV = gross tumor volume, CTV = clinical target volume, PTV_{xGy} = the percentage of planning target volume receiving xGy, PRV = planning organ at risk volume, NS = not significant.

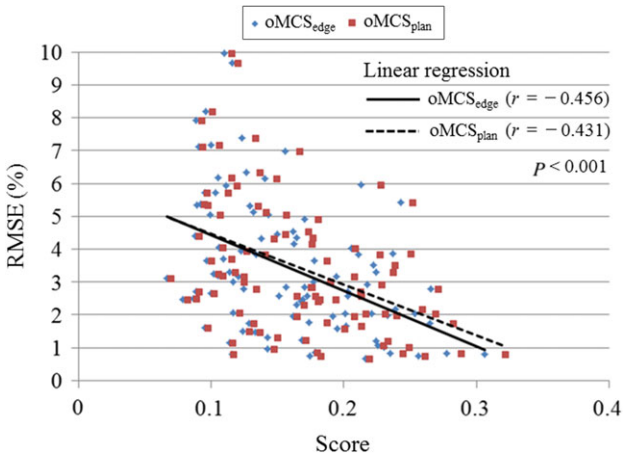

Fig. 4. Correlation between RMSEs and scores of $oMCS_{plan}$ or $oMCS_{edge}$ for the right parotid. Markers in blue represent $oMCS_{edge}$ and those in red represent $oMCS_{plan}$. The black solid lines and dotted lines are linear regressions for $oMCS_{edge}$ and $oMCS_{plan}$, respectively. The regression coefficient and associated P-value are shown.

concept and modified it in consideration of the organ location. We hypothesized the possibility of dose error where MLC leaves are more complex, which would create a steep gradient in intensity. In consideration of the organ location in the SI direction, we focused on the division of MCS according to the MLC leaf width. Using this approach, several organs were positioned at the same location in the SI direction. For example, both parotid grands and the spinal cord were present in the same slices in the SI direction (n = 3–7) (Fig. 1). To incorporate segment complexity for organs, particularly for the laterality of the beam's eye view, SEM was proposed and incorporated into the 3D grid, which corresponded to the dose grid from the DICOM RT-dose. Finally, it was confirmed that $oMCS_{edge}$ has a moderate negative correlation to RMSEs in the organs shown in Table 2 and Fig. 3. With regard to RMSEs for organs, the systematic errors in dose calculated under the QA setting may not be amenable to identification performed routinely, and it is difficult to make the systematic errors clear when these errors are small and are included in the random errors. Thus, it would be unknown whether the dose error was positive or negative. Therefore, RMSEs were used. If systematic changes derived from beam modeling, such as the MLC leaf transmission factor, leaf end transmission factor, beam penumbra width and beam output, had already been known, it could have affected the dosimetric impact directly and reconstructed the predicted dose as a systematic error [14]. The detector density of the 2D diode array may affect the dosimetric impact, especially for the small organ volumes [15]. It should be noted that the MGDR approach requires the TPS to be fully commissioned and a measurement device to be well calibrated [16]. If there are no differences among the planned and predicted doses using the perfect commissioned machine and TPS, $oMCS_{edge}$ may not be of much relevance; however, in reality, this may not always be practical. To minimize the uncertainty of dose delivery, QA is an ongoing imperative for maintaining the discrepancy within tolerance levels. The study we have conducted is compatible only with the Siemens machine; therefore, we should evaluate how $oMCS_{edge}$ works on other vendors' machines in the future.

In case a target requires a high dose but is anatomically contiguous to a critical organ (such as serial organs of the brain stem and spinal cord), PTV coverage may be poor if dose constraints are imposed. In such situations, $oMCS_{edge}$ can help estimate the dosimetric impact for the organs prior to beam delivery as the index can be calculated using the DICOM RT-plan file. In that case, the modification of the dose constraints of the spinal cord or brain stem would be required for guidance of a planning process by $oMCS_{edge}$. Consequently, if the $oMCS_{edge}$ were to be used as a simple index to be a part of pre-treatment evaluation of dose delivery, it would be expected that the index should be integrated with the TPS optimizer and/or leaf sequencer to mitigate the risk of low accuracy IMRT beams during a planning process.

In terms of the comparison of the correlation coefficients for $oMCS_{plan}$ and $oMCS_{edge}$, $oMCS_{edge}$ shows a stronger correlation with organs except for the GTV, the brain stem, the PRV brain stem, the spinal cord and the PRV spinal cord. It is likely that incorporating SEM into the $oMCS_{plan}$ is a valid method. As shown in Fig. 2c, the steep intensity gradient would be susceptible at the interface between the PTV and the OARs, such as the parotid glands. In contrast, there were almost no gradient in the case of the spinal cord. We have created the volume of interest for the brain stem and spinal cord as a PRV by the addition of 3-mm and 5-mm

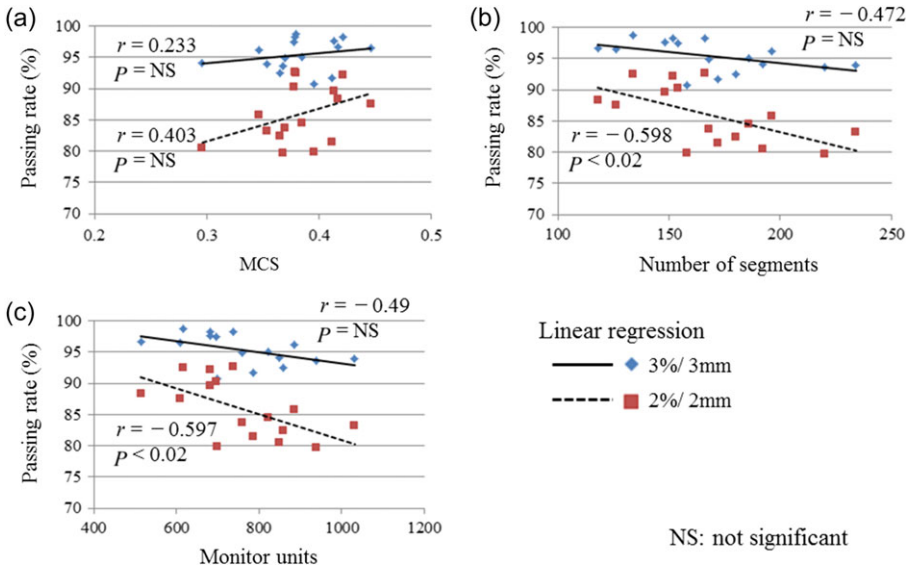

Fig. 5. Correlation between gamma passing rates under 3%/3 mm and 2%/2 mm criteria and MCS, the number of segments, and total monitor units in 16 cases. Markers in blue represent the 3%/3 mm criteria of gamma evaluation and those in red represent the 2%/2 mm criteria. The black solid lines and dotted lines are linear regressions for the 3%/3 mm and 2%/2 mm criteria of gamma evaluation, respectively. The regression coefficients and associated *P*-values are shown.

margins around each contour in 2D for dose optimization. As shown in Table 1, the $D_{2\%}$ of the PRV brain stem and that of the PRV spinal cord in the planned doses were 40.23 Gy and 41.38 Gy, respectively. Both planned doses were lower than the dose constraints, even when these organs were used as PRVs. Inevitably, the steep gradient in intensity seemed to be apart from the contours of these organs. This observation is very similar to the one reported by Manning *et al.* [17]. For the GTV, it is covered by the CTV in general. As Zhen *et al.* [14] have reported, the DVH curves for the GTV tend to be more condensed together than those for CTV and the OARs; there would be a relatively less steep gradient in intensity in the case of the GTV, which is likely to minimize dose errors.

For creation of the SEM, we used an edge width of 3-mm. The MLC leaf segmentation method used in this study employed the step-and-shoot technique, so that the change in intensity at the segment edge is rectangular-like. In case the beam delivery techniques are the sliding window and VMAT techniques, the change in intensity at the neighboring control point is smoother than that of the step-and-shoot technique. Therefore, an appropriate threshold for detecting and defining the different intensity as an edge should be found in the future; if so, a new factor might be necessary for considering the threshold in Eq. (7). Then, this proposed $oMCS_{edge}$ concept could be applied to any beam delivery technique. In other words, the threshold could affect the sensitivity of the correlation between the dose errors in the organs and the $oMCS_{edge}$.

The mean MCS from 16 cases in this study was 0.383; the corresponding value reported by McNiven *et al.* was 0.356 [3]. Both data were for H&N sites and employed step-and-shoot IMRT. Masi *et al.* [4] reported a mean MCS of 0.41 for different sites for VMAT delivery. Rajasekaran *et al.* [6] reported a mean MCS of 0.2224 for the H&N site using VMAT delivery. As for the correlation between gamma passing rates and MCS, no correlation was observed in the studies by McNiven *et al.* [3] and Rajasekaran *et al.* [6]. We also observed a similar tendency in our studies. As for the correlation between gamma passing rates and the number of segments and MUs is concerned, significant correlations with the correlation coefficient of −0.598 and −0.597 under 2% global/2 mm criteria shown in Fig. 5 were found. Wang *et al.* have reported the same significant correlation between the number of MUs and the gamma passing rate, even though the 2D gamma evaluation was under the criteria 1%/1 mm [18]. As Rajasekaran *et al.* [6] mentioned, beam complexity is not the only source that may contribute to dose errors, and by the incorporation of SEM into the $oMCS_{plan}$ ($oMCS_{edge}$), it was possible to correlate $oMCS_{edge}$ to the dose errors in the organs.

In conclusion, we have modified the original MCS concept that provides a complexity score to $oMCS_{edge}$ to include the organ location. Dose differences between the planned and predicted doses created by the MGDR approach were evaluated in the target and OARs. The proposed index of $oMCS_{edge}$ showed a moderate correlation to the dose errors in the organs. The index would guide plan modification to make the plan more robust against uncertainty. Future investigations should be performed to identify the cases in which the dose difference correlating with $oMCS_{edge}$ might result in random (positive and negative) errors and to find other parameters to improve the sensitivity of $oMCS_{edge}$. If the sensitivity of $oMCS_{edge}$ against the potential dose error for organs was higher and more correlated with periodical QA results, such as MLC leaf position accuracy and stability of beam profile, the index would allow a more relaxed patient-specific QA program.

CONFLICT OF INTEREST

There is no conflict of interest to declare.

REFERENCES

1. Low DA, Harms WB, Mutic S, et al. A technique for the quantitative evaluation of dose distributions. *Med Phys* 1998;25:656–61.
2. Harms WB Sr, Low DA, Wong JW, et al. A software tool for the quantitative evaluation of 3D dose calculation algorithms. *Med Phys* 1998;25:1830–6.
3. McNiven AL, Sharpe MB, Purdie TG. A new metric for assessing IMRT modulation complexity and plan deliverability. *Med Phys* 2010;37:505–15.
4. Masi L, Doro R, Favuzza V, et al. Impact of plan parameters on the dosimetric accuracy of volumetric modulated arc therapy. *Med Phys* 2013;40:071718.
5. Agnew CE, Irvine DM, McGarry CK. Correlation of phantom-based and log file patient-specific QA with complexity scores for VMAT. *J Appl Clin Med Phys* 2014;15:204–16.
6. Rajasekaran D, Jeevanandam P, Sukumar P, et al. A study on the correlation between plan complexity and gamma index analysis in patient specific quality assurance of volumetric modulated arc therapy. *Rep Pract Oncol Radiother* 2015;20:57–65.
7. Xu Z, Wang IZ, Kumaraswamy LK, et al. Evaluation of dosimetric effect caused by slowing with multi-leaf collimator (MLC) leaves for volumetric modulated arc therapy (VMAT). *Radiol Oncol* 2016;50:121–8.
8. Zhen H, Nelms BE, Tomé WA. Moving from gamma passing rates to patient DVH-based QA metrics in pretreatment dose QA. *Med Phys* 2011;38:5477–89.
9. Sumida I, Yamaguchi H, Kizaki H, et al. Three-dimensional dose prediction based on two-dimensional verification measurements for IMRT. *J Appl Clin Med Phys* 2014;15:133–46.
10. Younge KC, Matsuzak MM, Moran JM, et al. Penalization of aperture complexity in inversely planned volumetric modulated arc therapy. *Med Phys* 2012;39:7160–70.
11. International Commission on Radiation Units and Measurements. Prescribing, recording and reporting photon-beam intensity-modulated radiation therapy (IMRT). Special considerations regarding absorbed-dose and dose–volume prescribing and reporting in IMRT. ICRU Report 83. *J ICRU* 2010;10:27–40.
12. Sa'd MA, Graham J, Liney GP, et al. Quantitative comparison of 3D and 2.5D gamma analysis: introducing gamma angle histograms. *Phys Med Biol* 2013;58:2597–608.
13. Steiger JH. Tests for comparing elements of a correlation matrix. *Psychol Bull* 1980;87:245–51.
14. Zhen H, Nelms BE, Tomé WA. On the use of biomathematical models in patient-specific IMRT dose QA. *Med Phys* 2013;40:071702.
15. Keeling VP, Ahmad S, Algan O, et al. Dependency of planned dose perturbation (PDP) on the spatial resolution of MapCHECK 2 detectors. *J Appl Clin Med Phys* 2014;15:100–17.
16. Breen SL, Moseley DJ, Zhang B, et al. Statistical process control for IMRT dosimetric verification. *Med Phys* 2008;35:4417–25.
17. Manning MA, Wu Q, Cardinale RM, et al. The effect of setup uncertainty on normal tissue sparing with IMRT for head-and-neck cancer. *Int J Radiat Oncol Biol Phys* 2001;51:1400–9.
18. Wang J, Jin X, Peng J, et al. Are simple IMRT beams more robust against MLC error? Exploring the impact of MLC errors on planar quality assurance and plan quality for different complexity beams. *J Appl Clin Med Phys* 2016;17:147–57.